

STUDIES ON PLANAR ANTENNAS UTILIZING PATTERN DIVERSITY FOR MIMO WIRELESS APPLICATIONS

A DISSERTATION

*Submitted in partial fulfillment of the
requirements for the award of the degree
of*

INTEGRATED DUAL DEGREE

(Bachelor of Technology & Master of Technology)

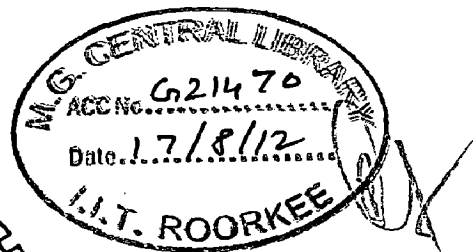
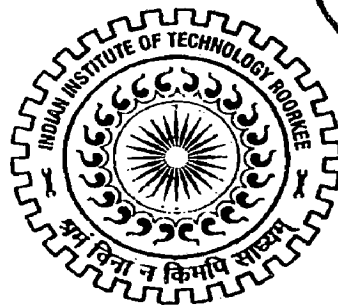
in

ELECTRONICS & COMMUNICATION ENGINEERING

(With Specialization in Wireless Communication)

By

NISCHEY GROVER



DEPARTMENT OF ELECTRONICS AND COMPUTER ENGINEERING
INDIAN INSTITUTE OF TECHNOLOGY ROORKEE
ROORKEE - 247 667 (INDIA)

JUNE, 2012

CANDIDATES DECLARATION

I hereby declare that the work being presented in the dissertation entitled, **Studies on Compact Planar Antennas Utilizing Pattern Diversity For MIMO Wireless Applications** in partial fulfillment of the requirements for the award of the degree of Integrated Dual Degree in Electronics and Communication Engineering, submitted in the Department of Electronics and Computer Engineering, Indian Institute of Technology Roorkee (India), is an authentic record of my own work carried out under the guidance of Dr. M.V. Kartikeyan, Professor, Department of Electronics and Computer Engineering, Indian Institute of Technology Roorkee. The matter embodied in the dissertation report has not been submitted for the award of any other degree elsewhere.

Date : 31 May 2012

Place : IIT Roorkee

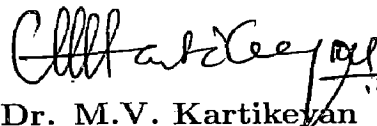

(Nischey Grover)

CERTIFICATE

This is to certify that the above statement made by the candidate is correct to the best of my knowledge.

Date : 31/05/2012

Place : IIT Roorkee


Dr. M.V. Kartikeyan
Professor
E&CE Department
IIT Roorkee

Acknowledgements

I would like to thank my supervisor **Dr. M.V. Kartikeyan** for his tremendous support and guidance. He is an inspiring professor, a great advisor and most of all, a really nice person. His sound guidance helped me out through various difficult situations during my stay in IIT Roorkee.

I would also like to thank my teachers **Dr. S.N. Sinha, Dr. D. Singh, Dr. A. Patnaik** and **Dr.N.P. Pathak** for strengthening my concepts in the field of wireless communications, RF and microwave engineering. It was their teachings which instilled a great interest in me for this topic.

I would also like to thank **Mr. Rajaram, Mr. Giri** and **Mr. Gaur** for their valuable support in fabrication and testing of the antennas designed in this thesis. I would also like to thank my friends **Mr. Ghanshyam, Mr. K. Shiva** , **Mr. Kumar Goodwill, Mr. Parth Kalaria** and my seniors **Mr. Jagannath Malik, Mr. Ashwini Arya** and **Mr. Arjun Kumar** for their tremendous guidance and encouragement.

Last but not the least, I would like to thank my family for providing me with a good environment for studies, which was essential for successfully carrying out this dissertation.


(Nischey Grover)

Abstract

Recent developments in wireless communications have shown that by using multiple antenna elements at both transmitter and the receiver, it is possible to substantially increase the capacity in a wireless communication system without increasing the transmission power and bandwidth. This system with multiple antenna elements at both link-ends is termed the MIMO (Multiple-Input Multiple-Output) system. The design of multiple antennas for handheld devices is a challenging task as it is very difficult to obtain a high degree of isolation between multiple antennas given the increasingly small dimensions of modern wireless terminals. Therefore novel antenna solutions need to be provided before MIMO technology can successfully be implemented on compact terminals. This dissertation aims to provide novel antenna solutions for the same.

Table of Contents

Acknowledgements	iii
Abstract	iv
Table of Contents	v
List of Tables	viii
List of Figures	ix
1 Introduction	1
1.1 Background	1
1.2 Motivation	2
1.3 Problem Statement	3
1.4 Methodology and Limitations	4
1.5 Outline of the dissertation	4
2 Basic Theory and Literature Review	6
2.1 Introduction	6
2.2 MIMO Systems	7
2.2.1 Array Gain	7
2.2.2 Diversity Gain	8
2.2.3 Spatial Multiplexing Gain	8
2.2.4 Interference Reduction	9
2.3 Channel Capacity	9
2.4 Signalling Schemes in MIMO Systems	12
2.4.1 Spatial Multiplexing	12
2.4.2 Space Time Coding	14
2.5 Antenna Diversity	15
2.5.1 Spatial Diversity	17

2.5.2	Pattern Diversity	18
2.5.3	Polarization Diversity	19
2.6	Performance Metrics for Evaluating MIMO Antennas	20
2.6.1	Correlation	20
2.6.2	Mean Effective Gain (MEG)	23
2.6.3	Mutual Coupling	24
2.6.4	Total Active Reflection Coefficient (TARC)	24
2.7	Pattern diversity based antennas	26
2.8	Multimode Antennas	27
2.9	Research Gaps Identified	34
3	Square-Ring Patch Antenna Utilizing Higher Order Modes for Pattern Diversity	36
3.1	Microstrip Patch Antennas and Cavity Model	36
3.2	Conceptual Design of The Proposed Antenna	38
3.3	Parametric Sweeps	39
3.3.1	Effect of patch length	39
3.3.2	Effect of square ring length	39
3.3.3	Effect of ring width keeping ring length constant	41
3.3.4	Effect of probe position	43
3.3.5	Effect of substrate	43
3.4	Results	44
3.5	Fabrication and Measurements	45
3.6	Analysis of the designed antenna	45
3.6.1	Antenna Covariance	45
3.6.2	Propagation Channel Model	49
3.6.3	MIMO Channel Capacity	50
3.6.4	Results	53
4	Size Reduction and Extension of Concept to Three Port Square Ring Patch Antenna Design	56
4.1	Introduction	56
4.2	Square ring at TM_{20} mode	56
4.3	Conceptual Design of the Antenna	58
4.4	Parameter sweeps	59
4.4.1	Effect of via radius	59
4.4.2	Effect of via position	60
4.4.3	Effect of ring width	60
4.5	Results	62

4.6	Analysis of the Designed Antenna	63
4.7	Extension to Three Port Square Ring-Patch Antenna	68
4.7.1	Analysis of the Designed Antenna	68
4.8	Further size reduction of three port square ring patch antenna using patch slots	71
4.8.1	Results	73
4.8.2	Analysis of the Designed Antenna	74
5	Conclusions and Future Scope	76
	Bibliography	79
	List of Publications	83

List of Tables

- 3.1 Optimized values of the design parameters 44
- 3.2 Capacity comparison for designed antenna with patch array 55

- 4.1 Optimized values of design parameters 62
- 4.2 Capacity comparison for designed antenna with patch array 66
- 4.3 Optimized values of the design parameters 73

List of Figures

2.1	A MIMO comprising N_T transmit antennas and N_R receive antennas [1]	8
2.2	A 2x2 MIMO system with a spatial multiplexing scheme [1]	13
2.3	A 2x2 MIMO system with a space-time coding scheme [1]	14
2.4	showing two signals are combined in a basic diversity receiver [1]	16
2.5	Diagram showing the effect of antenna spacing on correlation coefficient [1]	18
2.6	Configuration of dual $n = 3$ dominant mode patch antenna with center conductor. Patterns due to excitation of each feed are identical except for a rotation of 30° [2]	28
2.7	Geometry of the two-mode microstrip antenna proposed. In (b) dotted lines represent short-circuited walls, solid lines patch edges and black points the feeding probes.[3]	30
2.8	Simulated radiation patterns of the two-mode antenna in XZ plane for Modes TM_{01} and TM_{11} [3]	30
2.9	Geometry of a spiral antenna with voltage sources between the single arms of the spiral [4]	31
2.10	Geometry of a spiral antenna with voltage sources between the single arms of the spiral [4]	31
2.11	Dual-mode antenna with its Rat-Race coupler [5]	33
2.12	Current distributions of (a) TM_{20} mode with a common feeding and (b) TM_{21} mode with a differential feeding [5]	33

2.13	The four port antenna design proposed in [6].	34
2.14	Variation of Envelope Correlation Coefficient with XPR [6].	35
3.1	Fundamental-mode electric-field configuration underneath a rectangular patch [7].	37
3.2	Fringing fields for fundamental-mode TM_{10} and higher order mode TM_{02} [7].	38
3.3	Microstrip patch radiation source represented by two equivalent slots [7].	38
3.4	Design of the proposed antenna along with design parameters (white represents copper and grey represents substrate)	40
3.5	(a) E-field distribution of surrounding square ring operating in TM_{22} mode.(b) Electric field distribution of central square patch operating in TM_{10} mode.	40
3.6	(a) farfield gain pattern (in linear scale) of square ring operating in TM_{22} mode (b) farfield gain pattern (in linear scale) of central patch operating in TM_{10} (fundamental) mode	41
3.7	Effect on ring length on resonant frequency of TM_{22} mode	42
3.8	Effect on ring width on resonant frequency of TM_{22} mode	42
3.9	Effect of substrate ϵ_r on resonant frequencies of various modes	43
3.10	Simulated S parameters of the designed antenna	44
3.11	: S parameters of the fabricated antenna measured on a VNA. clockwise from top left (a) S parameters of square ring indicating resonant frequency of TM_{22} mode at 3.6996GHz (b) S parameters of central square patch resonating in fundamental mode at 3.8825GHz. (c) and (d) represent mutual coupling which is well below -25dB	46
3.12	Image of the fabricated TM_{22} Square Ring Patch Antenna	47
3.13	(a) E plane farfield pattern of central patch (b) H plane farfield pattern of central patch(In linear scale)	47

3.14	Radiation patterns of TM_{22} ring (a) XZ plane (b) YZ plane(In linear scale)	48
3.15	Patch array for 3.5 GHz with half wavelength separation for spatial diversity	54
3.16	Cumulative capacity distribution. (red line shows CCDF of SISO system, blue line shows CCDF of 2X2 MIMO System using designed antenna and Dotted blue line shows the CCDF of 2X2 MIMO System using patch array)	55
4.1	Radiation pattern (top) and corresponding surface current distribution (below) of square ring with (a) very less inner gap and (b) as inner gap is increased	57
4.2	Electric field distribution in TM_{20} square ring	58
4.3	Design of the proposed Square Ring Patch Antenna (hollow circles indicate vias and solid circles indicate feed location)	59
4.4	Effect of via radius on resonant frequency of TM_{20} mode of square ring	60
4.5	Effect of via position on resonant frequency of TM_{20} mode of square ring	61
4.6	Effect of ring width on resonant frequency of TM_{20} mode of square ring keeping via position constant w.r.t. inner edge	61
4.7	Simulated S-parameters for the designed Square Ring Patch Antenna	62
4.8	Fabricated Square Ring Patch Antenna (front and back sides)	63
4.9	S parameters of fabricated antenna on VNA. clockwise from top left (a) S parameters of square ring indicating resonant frequency of TM_{20} mode at 3.5021GHz (b) S parameters of central square patch resonating in fundamental mode at 3.6597GHz. (c) and (d) represent mutual coupling which is well below -20dB	64
4.10	(a) E plane farfield pattern of central patch (b) H plane farfield pattern of central patch(In linear scale)	65

4.11 (a) Measured farfield gain patterns of TM_{20} ring in XZ plane (b) in YZ plane (In linear scale)	65
4.12 Capacity CCDF for different cases. (red line shows CCDF of SISO system, Blue line shows CCDF of 2X2 MIMO System using designed antenna and Dotted blue line shows the CCDF of 2X2 MIMO System using patch array)	67
4.13 3 port square ring patch antenna	69
4.14 E field distribution for different modes in the proposed Square Ring Patch Antenna	69
4.15 Simulated S parameters for three port square ring patch antenna	70
4.16 CCDF for the designed three port antenna (dotted line represents CCDF of-patch array while solid line represents CCDF of designed antenna)	71
4.17 Square ring patch with slots	72
4.18 Farfield pattern of (a) square ring (feed 1) (b) patch (feed 2) (c) patch(feed 3) (linear scale)	72
4.19 Simulated S-parameters of the designed antenna.	73
4.20 CCDF for the designed three port antenna (dotted line represents CCDF of-patch array while solid line represents CCDF of designed antenna)	75

Chapter 1

Introduction

1.1 Background

In the next generation of mobile communication systems there is a need for higher performance of the mobile terminals, accomplished by higher data rates and better quality of service. Over the last two decades, the use of mobile communication technology has experienced a significant growth from first-generation (1G) analog voice-only communication to second-generation (2G) digital voice communication. Currently, the third generation (3G) mobile communication technology not only provides digital voice services, but also provides video telephony, internet access and download services. Further, the forthcoming standards like WiMAX , LTE etc aim to provide even higher data rates and longer range to provide quality services to end users. In order to achieve this, wireless communication technology has to be pushed to the physical limits of the radio channels. A well known upper bound on the maximum achievable data rate for the ideal band-limited additive white Gaussian noise (AWGN) channel is the Shannon-Nyquist criterion [8]. Having an available channel bandwidth, W and signal-to-noise ratio (SNR) over this bandwidth, the maximum

them. While coding and signal processing are key elements to successful implementation of a MIMO system, the propagation channel and antenna design represent major parameters that ultimately impact system performance. As a result, considerable research has been devoted recently to these two areas. MIMO systems perform best when the correlation between signals on the different antennas is low [13]. Antenna properties such as pattern, polarization, array configuration, and mutual coupling can impact this correlation. It is a very challenging task to accommodate multiple antennas with low correlation given the small dimensions of mobile terminals. Conventionally, low correlation can be achieved at the base stations by spacing the antennas an appropriate distance apart, ideally half wavelength distance. This is called spatial diversity. However, at mobile terminals, the space is very limited and the antennas cannot be placed too far apart, this will result in high correlation which would degrade MIMO performance. Pattern and polarization diversities are an elegant way of obtaining uncorrelated signals in a multipath environment by utilizing orthogonal patterns and polarizations respectively. Therefore pattern and polarization diversity based MIMO systems are suitable for implementation on a compact wireless terminal. This dissertation aims to design and analyze some compact designs utilizing pattern diversity for MIMO wireless communications on a compact terminal.

1.3 Problem Statement

This dissertation aims to propose novel compact planar microstrip antenna solutions utilizing pattern diversity concept for MIMO applications. Using higher order resonating modes of an antenna for obtaining uncorrelated patterns is an attractive

detailed literature review of pattern diversity based antennas is done with emphasis on multimode antennas. In Chapter 3 a two port square ring patch antenna is designed and related theory is given. Further a detailed analysis in terms of capacity, correlation and mean effective gain of designed antenna is performed. MIMO Antenna Design Suite v1 is developed which is set of MATLAB programs for computing the necessary parameters for evaluating MIMO Antennas. In chapter 4 the antenna designed chapter 3 is modified for operation at a different set of modes which leads to overall size reduction. Further the concept of orthogonal polarization diversity is used to extend the design to accommodate an extra port, leading to a three port compact antenna design. Further, a detailed MIMO analysis is done using method described in chapter 3. Chapter 5 concludes the dissertation.

2.2 MIMO Systems

In a conventional radio system, there is only one antenna between transmitter and receiver. This system is called a Single Input Single Output (SISO) System. The capacity of such systems is limited by Shannon-Nyquist Criterion [8]. As mentioned in Chapter 1, future wireless mobile services demand much higher data bit-rate transmission. In order to increase the capacity of the SISO systems to meet such demand, the bandwidth and transmission power have to be increased significantly. Recent developments have shown that using MIMO (Multiple-Input Multiple-Output) systems could substantially increase the capacity in wireless communication without increasing the transmission power and bandwidth [10],[11]. Rayleigh fading caused by multipath has been a source of problem for conventional wireless systems. However MIMO systems exploit multipath instead of mitigating it. MIMO wireless systems have demonstrated the potential for increased capacity in rich multipath environments. Such systems operate by exploiting the spatial properties of the multipath channel, thereby offering a new dimension which can be used to enable enhanced communication performance. A typical MIMO system is shown in Figure 2.1

The performance improvements resulting from the use of MIMO systems are due to array gain, diversity gain, spatial multiplexing gain, and interference reduction [9]. A brief description of these is given below:

2.2.1 Array Gain

Array gain can be made available through processing at the transmitter and the receiver and results in an increase in average receive SNR due to a coherent combining effect [9].

2.2.4 Interference Reduction

When multiple antennas are used, the differentiation between the spatial signatures of the desired signal and interference signals can be exploited to reduce interference. Interference reduction requires knowledge of the desired signal's channel. Exact knowledge of the interferer's channel may not be necessary [9].

2.3 Channel Capacity

Figure 2.1 shows a MIMO system with N_T transmit antennas and N_R receive antennas. For a narrowband channel, the complex transmission coefficient between element $k \in [1, \dots, N_T]$ at the transmitter and element $j \in [1, \dots, N_R]$ at the receiver at time t is represented by $h_{jk}(t)$. A matrix containing all channel coefficients (channel coefficient matrix, $H(t)$) can be shown as:

$$H(t) = \begin{pmatrix} h_{1,1}(t) & h_{1,2}(t) & \cdots & h_{1,N_T}(t) \\ h_{2,1}(t) & h_{2,2}(t) & \cdots & h_{2,N_T}(t) \\ \vdots & \vdots & \ddots & \vdots \\ h_{N_R,1}(t) & h_{N_R,2}(t) & \cdots & h_{N_R,N_T}(t) \end{pmatrix} \quad (2.3.1)$$

Hence, a system transmitting the signal vector $x(t) = [x_1(t), x_2(t), \dots, x_{N_T}(t)]^T$, where $x_k(t)$ is the signal transmitted from the k^{th} antenna would result in the signal vector $y(t) = [y_1(t), y_2(t), \dots, y_{N_R}(t)]^T$ being received, where $y_j(t)$ is the signal received by the j^{th} antenna, and

$$y(t) = H(t)x(t) + n(t) \quad (2.3.2)$$

the Shannon channel capacity will be

$$C = \log_2(1 + \rho) \quad (2.3.5)$$

Where ρ is the receiver SNR. If the transmit power is instead equally divided among the lines, the capacity becomes [13]:

$$C_Q = \sum_{q=1}^Q \log_2(1 + \rho/Q) = Q \log_2(1 + \rho/Q) \quad (2.3.6)$$

Where equal receiver noise is assumed. For a transmit vector whose elements are complex Gaussian-distributed random variables, the expression for channel capacity is [13]:

$$C = \max_{R_x: Tr(R_x) \leq P_t} \log_2 \left| I + \frac{H R_x H^H}{\sigma^2} \right| \quad (2.3.7)$$

Where $R_x = E(xx^H)$ is the transmit covariance matrix. The diagonal elements of R_x represent transmit power from each antenna and hence the constraint $Tr(R_x) \leq P_t$ where P_t is the total transmit power. Determining the capacity involves identifying the covariance matrix R_x that maximizes Eqn. 2.3.7. However when the transmitter does not know H , it can equally divide the power among the transmit antennas to form N_T independent streams or $R_x = (P_T/N_T)I$. Thus the uninformed transmit capacity is given by [13],

$$C_{UT} = \log_2 \left| I + \frac{P_T H H^H}{N_T \sigma^2} \right| \quad (2.3.8)$$

which may be decomposed as [9]:

$$C_{UT} = \sum_{i=1}^r \log_2 \left(1 + \frac{P_T \lambda_i}{N_T \sigma^2} \right) \quad (2.3.9)$$

Where r is the rank of H and λ_i ($i=1$ to r) are the positive eigenvalues of $H H^H$. It can be seen from Eqn. 2.3.9 that multiple scalar spatial data pipes (also known

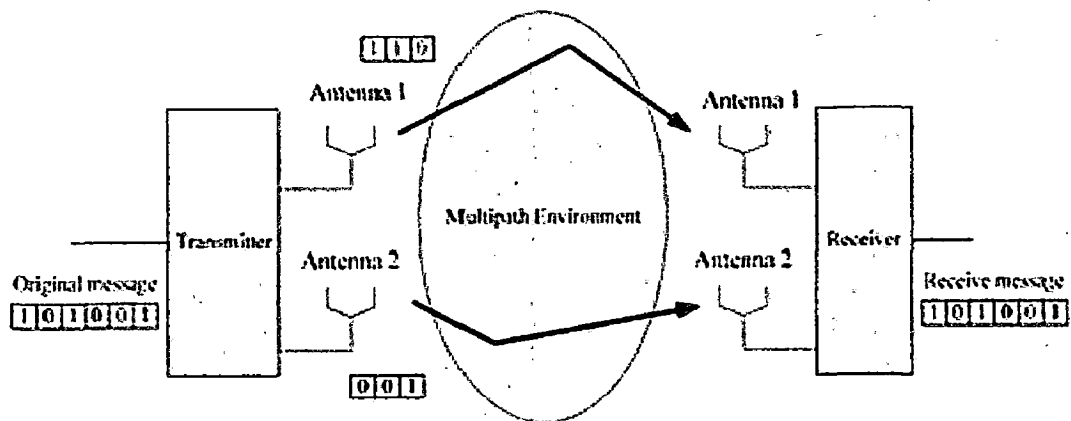


Figure 2.2: A 2x2 MIMO system with a spatial multiplexing scheme [1]

that the receiver has knowledge of the channel, it can differentiate between the co-channel signals and extract both signals. After demodulating the received signals, the original sub streams can be combined to yield the original bit stream of data. Therefore, spatial multiplexing leads to increase in the channel capacity with the number of transmit-receiver antenna pairs. This concept can be extended to more general MIMO channels.

The maximum number of parallel channels that can be achieved in an ideal MIMO system is $\min(N_T, N_R)$. Shannon's capacity formula for SISO system indicates that in the high SNR regime, a 3dB increase in SNR will approximately increase capacity by 1 bit/s/Hz. However, in the MIMO systems, the capacity in the high SNR regime will increase by $\min(N_T, N_R)$ bits/s/Hz with every increment of 3dB in SNR. However, SM does not work well in low SNR environments as it is more difficult for the receiver to identify the uncorrelated signal paths [1].

linearly with the number of transmit/receive elements used. However, it maximizes the wireless range and coverage by improving the quality of the transmission. In order to improve both range and capacity, a MIMO implementation requires to support both the SM and space-time coding schemes. Examples of diversity coding techniques are the Alamouti scheme and delay diversity.

2.5 Antenna Diversity

Multipath propagation had historically been regarded as an impairment because it causes signal fading. In order to mitigate this problem, diversity techniques were developed. The basic principle of diversity is that the receiver should have more than one version of the transmitted signal available, where each version is received through a different uncorrelated channel. These versions of transmitted signal are combined appropriately to give signal with higher mean SNR at the output compared to a single branch resulting in a diversity gain.

Fig. 2.4 shows that a dual-element diversity antenna at a receiver can receive two different versions of transmitted signals and combine them with a combiner circuit. There are three kinds of diversity combining techniques (i) Selection diversity chooses the path with the highest SNR, and performs detection based on the signal from the selected path. (ii) Maximal ratio combining (MRC) makes decisions based on an optimal linear combination of the path signals. (iii) Equal gain combining (EGC) simply adds the path signals after they have been co-phased [14].

MIMO systems exploit the channel spatial degrees of freedom to increase communication performance. In traditional antenna diversity, these resources are used to transmit and/or receive duplicate copies of a single information stream to increase

techniques can be applied to obtain uncorrelated signals and therefore can be used to design MIMO antennas. The following subsections describe these antenna diversities in detail.

2.5.1 Spatial Diversity

In spatial diversity more than one antenna are employed which are sufficiently separated from each other so that the relative phases of the multipath contributions are significantly different at the two antennas. When large phase differences are present, they give rise to a low correlation between the signals at the antennas.

By assuming a two dimensional scenario wherein angular density function is taken to be uniform in azimuth of the mobile environment and no angular density function in elevation, the correlation coefficient for a distance separation d can be obtained from the zeroth order Bessel function, $J_0(x)$ [1].

$$\rho_{12} = J_0(\beta d) \quad (2.5.1)$$

Where β is the phase constant. The first null of $J_0(\beta d)$ is at $d = 0.4\lambda$, as shown in Fig. 2.5. As shown graphically in Fig. 2.5, the correlation coefficient starts to increase after $d = 0.4\lambda$. However, in suburban areas the measurements show that the first null appears at about $d = 0.8\lambda$ [1]. This may be due to a lack of uniform angular distribution of wave arrival. Generally, spacing, d of 0.5λ is practically used to obtain two uncorrelated signals at mobile terminals [1].

correlation) [16]. Finding other antenna topologies that offer this orthogonality in a compact form remains an area of active research. In this dissertation the concept of multimode antennas has been explored to provide novel compact planar antenna solutions for pattern diversity.

2.5.3 Polarization Diversity

Recent work has suggested that in a rich multipath environment, sensing the three Cartesian vector components of the electric and magnetic fields can provide six uncorrelated signals at the receiver. With the use of polarization diversity the size of the antenna structure can be reduced significantly. Polarization diversity can potentially lead to low correlation on at least two branches even when the channel is characterized by little or no multipath scattering [7].

To understand the fundamentals of polarization diversity in MIMO systems, consider two dipoles that are rotated by angle α against one another, are used at the transmitter and at the receiver. Both transmit antennas radiate the same power. For increasing α capacity increases, since the correlation among the channel coefficients of H (the channel matrix) decreases. For $\alpha = 90^\circ$, the capacity is maximum as two different channels for two different polarizations exist. Those channels are coupled by cross polarization coupling and are not necessarily orthogonal sub channels.

The correlation among the two signals is not only influenced by polarization diversity, but also by pattern diversity. Polarization and pattern diversity are always combined and can not be exploited separately [17].

$$\rho_{12} = \frac{\int_0^\pi \int_0^{2\pi} (XPR \cdot E_{\theta 1}(\theta, \phi) E_{\theta 2}^*(\theta, \phi) P_\theta(\theta, \phi) + E_{\phi 1}(\theta, \phi) E_{\phi 2}^*(\theta, \phi) P_\phi(\theta, \phi)) \sin\theta d\phi d\theta}{\sqrt{\sigma_1^2 \sigma_2^2}} \quad (2.6.2)$$

Where σ_n^2 is the variance of branch n

$$\sigma_n^2 = \int_0^\pi \int_0^{2\pi} (XPR \cdot E_{\theta n}(\theta, \phi) E_{\theta n}^*(\theta, \phi) P_\theta(\theta, \phi) + E_{\phi n}(\theta, \phi) E_{\phi n}^*(\theta, \phi) P_\phi(\theta, \phi)) \sin\theta d\phi d\theta \quad (2.6.3)$$

Where XPR is the ratio of time averaged vertical power to time average horizontal power in the fading environment in linear form [1]:

$$XPR = \frac{P_V}{P_H} \quad (2.6.4)$$

where P_V is the average vertical power and P_H is the average horizontal power. XPR is also referred to as the cross-polarization power ratio or cross-polar discrimination (XPD). Both antennas in Eqn 2.6.2 have E-fields, $E_{\theta n}$ and $E_{\phi n}$ [Vm^{-1}]. $P_\theta(\theta, \phi)$ and $P_\phi(\theta, \phi)$ are the angular density function of the vertical and horizontal plane respectively. For reference, θ is the angle relative to the vertical axis z and ϕ is the angle in the horizontal plane.

The second type of correlation metric is the envelope correlation, ρ_e which is the correlation between two signal envelopes without considering the phase [1]:

$$\rho_e = \frac{\int_0^T (\sqrt{R_1^2(t)} - E(\sqrt{R_1^2})) (\sqrt{R_2^2(t)} - E(\sqrt{R_2^2})) dt}{\sqrt{\int_0^T (\sqrt{R_1^2(t)} - E(\sqrt{R_1^2}))^2 dt \int_0^T (\sqrt{R_2^2(t)} - E(\sqrt{R_2^2}))^2 dt}} \quad (2.6.5)$$

Where $R_1^2(t)$ and $R_2^2(t)$ are the square envelope [V^2] of $v_1(t)$ and $v_2(t)$ respectively (i.e. $|v_1(t)|^2$ and $|v_2(t)|^2$) Envelope correlation (ρ_e) is always real as the phase is not defined. It is assumed that with independent Gaussian sources the envelope

2.6.2 Mean Effective Gain (MEG)

As previously mentioned the mean power levels in various branches must be similar otherwise the weaker antenna may not be useful even if it is less faded. This criterion is mathematically expressed in terms of mean effective gain (MEG). Like correlation coefficient, MEG is very much dependant on distribution of incoming wave and orientation relative to radio environment. It is defined in [22] as the ratio between the mean received power of the antenna and the total mean incident power. The MEG is a figure of merit for the average performance of an antenna on a mobile terminal taking into account the incident radio wave distribution in the multipath environment and the gain patterns of the antenna. This parameter determines how effective the antenna will be in a multipath environment. The following equation has been derived in [22] for MEG:

$$MEG = \int_0^\pi \int_0^{2\pi} \left(\frac{XPR}{XPR+1} G_\theta(\theta, \phi) P_\theta(\theta, \phi) + \frac{1}{XPR+1} G_\phi(\theta, \phi) P_\phi(\theta, \phi) \right) \sin\theta d\phi d\theta \quad (2.6.8)$$

Where $G_\theta(\theta, \phi)$ and $G_\phi(\theta, \phi)$ are the θ and ϕ components of the antenna power gain patterns respectively. $P_\theta(\theta, \phi)$ and $P_\phi(\theta, \phi)$ are the θ and ϕ components of the angular density functions respectively as used in Eqn. 2.6.2. In order to have similar mean power levels, the ratio of MEG of two antennas must be close to unity i.e.

$$\frac{MEG_1}{MEG_2} \cong 1 \quad (2.6.9)$$

antenna operating band because TARC accounts for both coupling and random signal combining. TARC is calculated as the square root of the incident power provided by all excitations minus the radiated power and then dividing by the incident power [7]. The TARC at N port antenna can be described as [24]:

$$\Gamma'_a = \frac{\sqrt{\sum_{i=1}^N |b_i|^2}}{\sqrt{\sum_{i=1}^N |a_i|^2}} \quad (2.6.11)$$

where a_i is incident signal, and b_i is reflected signal. In case of 2X2 antenna arrays, the scattering matrix can be described as :

$$\begin{pmatrix} b_1 \\ b_2 \end{pmatrix} = \begin{pmatrix} S_{11} & S_{12} \\ S_{21} & S_{22} \end{pmatrix} \begin{pmatrix} a_1 \\ a_2 \end{pmatrix} \quad (2.6.12)$$

It is assumed that signal will be randomly phased with independent and identically distributed (i.i.d) Gaussian random variable because MIMO channels are assumed as Gaussian and multi-path spread in the propagation channel. Since sum or subtraction of independent Gaussian random variable is also gaussian, reflected signals are characterized as:

$$b_1 = S_{11}a_1 + S_{12}a_2 = S_{11}a_0e^{j\theta_1} + S_{12}a_0e^{j\theta_2} = a_1(S_{11} + S_{12}e^{j\theta}) \quad (2.6.13)$$

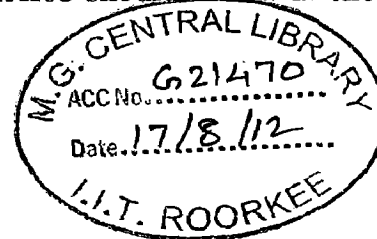
$$b_2 = S_{21}a_1 + S_{22}a_2 = S_{21}a_0e^{j\theta_1} + S_{22}a_0e^{j\theta_2} = a_1(S_{21} + S_{22}e^{j\theta}) \quad (2.6.14)$$

Therefore, TARC is described as follows;

$$\Gamma'_a = \sqrt{\frac{|a_1(S_{11} + S_{12}e^{j\theta})|^2 + |a_1(S_{21} + S_{22}e^{j\theta})|^2}{\sqrt{2}|a_i|^2}} \quad (2.6.15)$$

$$= \sqrt{\frac{(S_{11} + S_{12}e^{j\theta})^2 + (S_{21} + S_{22}e^{j\theta})^2}{\sqrt{2}}} \quad (2.6.16)$$

Using Eqn. 2.6.15 TARC for 2X2 antenna array can be directly calculated from the scattering matrix. TARC can be used as an alternative criterion to define the multiport antenna operating band. Thus TARC should be low in the operating band [25].



a decoupling network in the receiver by splitting two orthogonal radiation modes. In this way, good isolation between the sum and difference ports (the input ports of the system) of the coupler is obtained which is critical to the MIMO system performance.

Introducing antenna arrays and parasitic elements at both the transmitter and receiver will undoubtedly increase the cost of producing the terminals. Furthermore, fitting several elements onto a small handset is not very feasible. An interesting antenna solution, which appears well suited for MIMO systems, is the multimode antenna. The multimode antenna offers characteristics similar to those of an antenna array through multiple modes, but using only a single antenna element. The physical mechanism that yields different received signals is the fact that each mode has a different radiation pattern and two nearly orthogonal radiation patterns can behave as two separate antennas. Thus, using a multimode antenna to achieve diversity can be seen as a special kind of pattern diversity [16]. The topic of multimode antennas would be discussed in a greater detail in the next section.

2.8 Multimode Antennas

A multimode antenna is an antenna where several modes are excited separately on the same antenna structure. Essentially, different modes represent different solutions to Maxwell's equations that fulfill the boundary conditions for the given geometry. Several modes or solutions can exist at the same time on the same structure. In fact, it is possible to excite several modes at the same temporal frequency on one antenna structure separately, and regard these as separate antenna ports. The concept of multimode antennas for diversity applications was first introduced in [2] where a two port circular patch antenna is operated in higher order modes to extract pattern diversity.

Where k_0 is the free space propagation constant, ϕ_0 is the reference angle which corresponds to peak magnetic current V_0 and $J_n = J_n(k_0 a \sin \theta)$.

For the mobile communications case, where the source region is omnidirectional, any different azimuthal modes n_1 and n_2 where $n_1 \neq n_2$ will have low correlation. Furthermore, any nonzero azimuthal mode n when rotated by $\pi/(2n)$ will be orthogonal to its unrotated form. This means that the same mode can be used to provide two radiation patterns which are orthogonal; i.e., two-branch diversity is available from the same azimuthal mode by exciting it as an orthogonal degenerate pair. The farfield radiation patterns of $n=3$ dominant mode is shown in Fig 2.6. It can be seen from the figure that a rotation by 30 degrees has resulted in an orthogonal pattern. The radius of the central conductor can be used to change the resonant frequency of $n=0$ mode so that it is well away from frequency of interest in order to reduce mutual coupling between the two antenna ports.

Another example of multimode antenna is given in [3] where a compact short circuited ring patch as shown in is utilized to obtain orthogonal radiation patterns. The design is shown in Fig. 2.7. The design is a two-mode microstrip patch antenna made with a short-circuited ring patch operated at TM_{01} mode and a circular patch (CP) working at TM_{11} mode. TM_{01} mode has its radiation maximum in the plane containing the antenna with a rotational symmetry radiation pattern and a null in the broadside direction whilst TM_{11} mode has always a maximum in the broadside direction. Consequently, these two modes can be considered orthogonal. TM_{01} being the fundamental mode of a SCRPA antenna its size is comparable to the CP operated at TM_{11} mode. Fig 2.8 shows the radiation patterns of two modes.

A wideband multimode antenna for pattern diversity based on four arm spiral

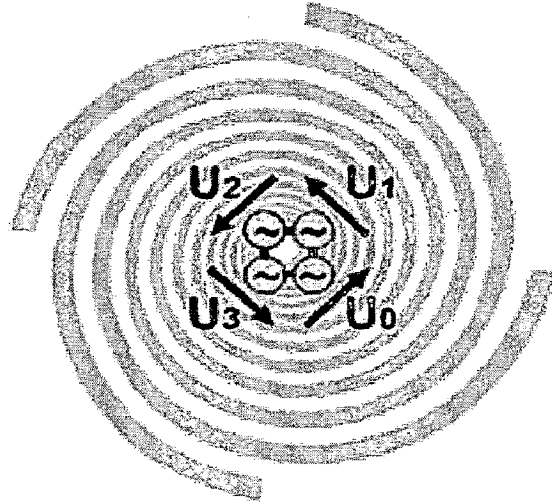


Figure 2.9: Geometry of a spiral antenna with voltage sources between the single arms of the spiral [4]

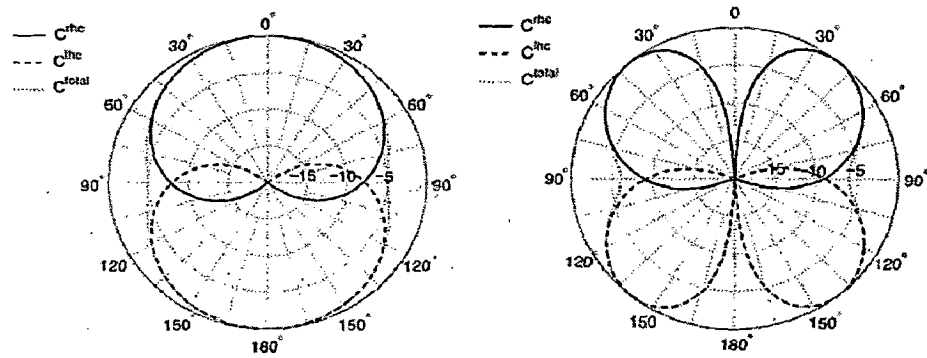


Figure 2.10: Geometry of a spiral antenna with voltage sources between the single arms of the spiral [4]

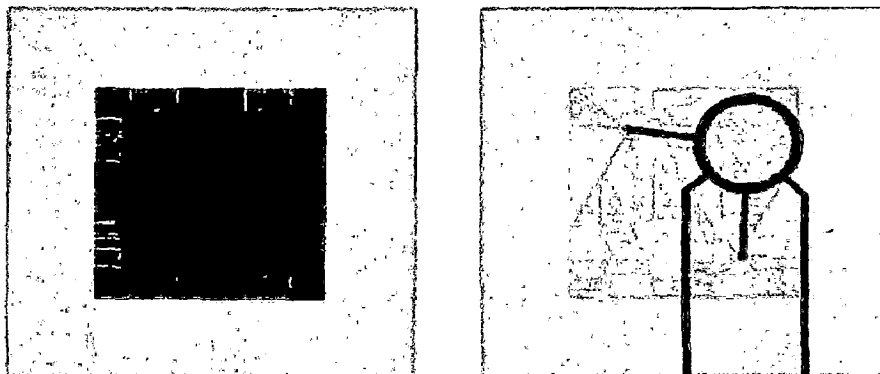


Figure 2.11: Dual-mode antenna with its Rat-Race coupler [5]

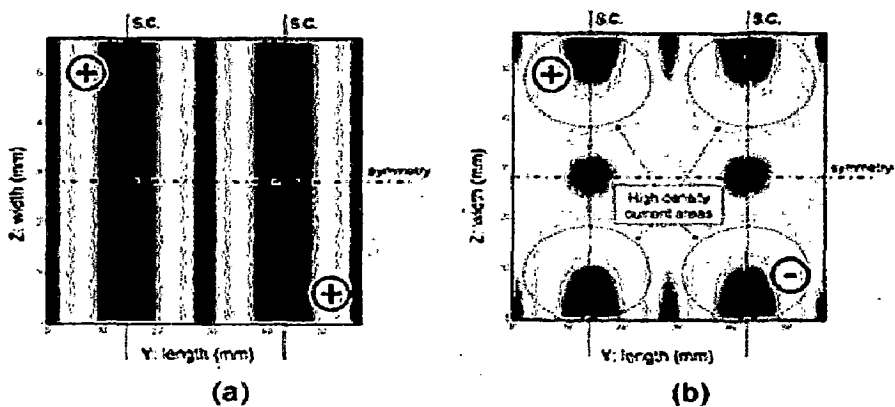


Figure 2.12: Current distributions of (a) TM_{20} mode with a common feeding and (b) TM_{21} mode with a differential feeding [5]

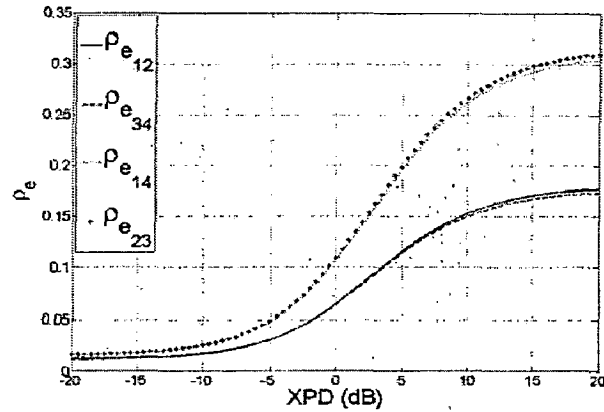


Figure 2.14: Variation of Envelope Correlation Coefficient with XPR [6].

- Novel antenna solutions need to be provided which are compact and planar.
- A four port antenna based on square ring patch geometry has been studied in [6] wherein a central patch antenna is excited in its fundamental TM_{10} mode and surrounding square ring is operated in TM_{21} mode.
- Since the radiation patterns of both modes are broadside therefore there is high correlation (~ 0.3) under certain environmental conditions as shown in Fig. 2.14.
- Therefore in this dissertation, the square ring patch antenna is studied in order to improve the correlation properties using pattern diversity.

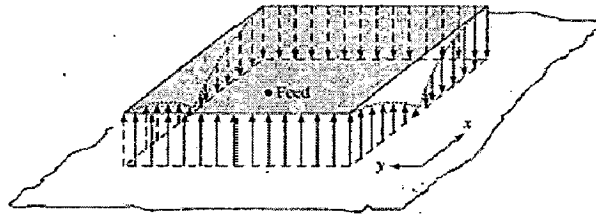


Figure 3.1: Fundamental-mode electric-field configuration underneath a rectangular patch [7].

a completely enclosed metallic cavity.

For a rectangular or square patch with relative dielectric constant ϵ_r , substrate thickness h , and patch dimensions $L \times W$, the total electric field in the cavity can be expressed as the sum of the fields associated with each sinusoidal mode [30]:

$$E_z(x, y) = \sum_m \sum_n C_{mn} \cos\left(\frac{m\pi}{L}x\right) \cos\left(\frac{n\pi}{W}y\right) \quad (3.1.1)$$

where C_{mn} is a constant that depends on the feed location, L and W dimensions. Due to the very thin substrate, the fields are assumed to be z -directed only, with no variation in the z -direction. The dominant mode is the TM_{10} mode, which could be obtained if the dimension L is approximately $\lambda_g/2$ (λ_g is the effective wavelength in the dielectric). The field variation underneath the patch for this fundamental mode is illustrated in Fig. 3.1, and the radiating fringing fields are shown in Fig. 3.2. These figures indicate that, along the central line orthogonal to the resonant direction (x -direction); it is a null field region underneath the patch. This is why one can place shorting pins or additional feed probes along this central line without disturbing the performance of the patch of the original feed. This is also why two orthogonally placed feed probes can achieve dual-linear polarization without much mutual coupling.

In Fig. 3.2, the left- and right-edge fringing fields do not contribute much to far fields since they cancel each other in the far field. The top- and bottom-edge

patch is operated in the fundamental mode i.e. TM_{10} (for reference x and y axis are mentioned in Fig. 3.4).

Central patch's E-field distribution is shown in Fig. 3.5(b). The surrounding ring is operated in a higher order mode. The antenna is designed to operate at center frequency of 3.5 GHz. Both the square ring and patch should therefore resonate in their respective modes at 3.5 GHz. Therefore the aim of the design process is to converge the resonance frequencies of respective modes of both the square patch and the square ring. Here the ring is chosen to be excited in TM_{22} mode since its radiation pattern is nearly orthogonal to fundamental mode of patch, such that low correlation can result. Also the ring dimension for TM_{22} mode is larger enough to accommodate a central square patch. The E-field distribution of the surrounding square ring for TM_{22} mode is shown in Fig. 3.5(a). Farfield radiation patterns shown in Fig. 3.6 indicate orthogonal channels.

3.3 Parametric Sweeps

3.3.1 Effect of patch length

Resonant frequency of fundamental mode of patch decreases with patch length. This is because of increase of electrical size of the patch as described in cavity model in previous section.

3.3.2 Effect of square ring length

Keeping width of square ring constant the length of square ring is varied to see its effect on resonant frequency of TM_{22} mode. As shown in Fig. 3.7 it is found that

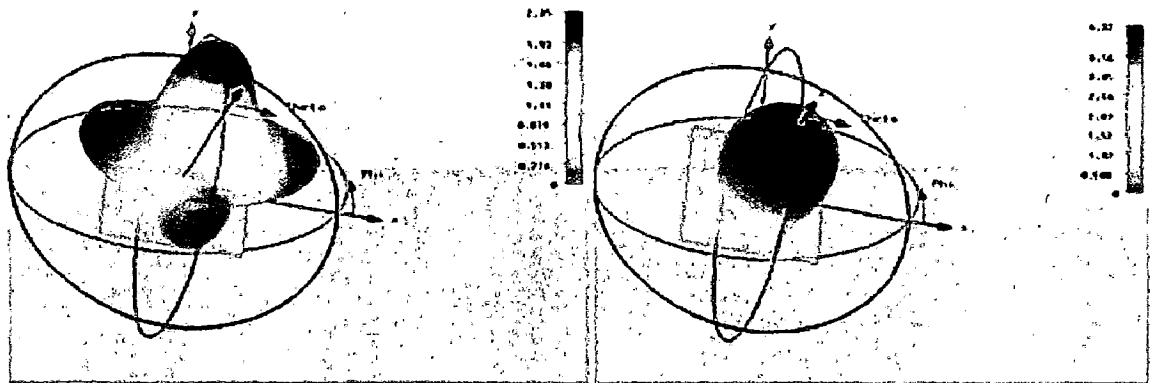


Figure 3.6: (a) farfield gain pattern (in linear scale) of square ring operating in TM_{22} mode (b) farfield gain pattern (in linear scale) of central patch operating in TM_{10} (fundamental) mode

resonant frequency decreases with increase in length. This is because of increase in electrical size of the antenna with increase in dimension. Note that the other resonating modes just before and after TM_{22} mode in terms of resonant frequency have broadside patterns and therefore would not have led to appreciable diversity gain.

3.3.3 Effect of ring width keeping ring length constant

As seen from Fig. 3.8 with increase in ring width resonant frequency of TM_{22} mode decreases. However as can be seen from the figure the mode frequencies of TM_{22} and TM_{21} begin to converge with increase in width. Since TM_{21} mode has a broadside pattern it is desirable to not to allow these mode frequencies to converge so that orthogonality with square patch's pattern can be maintained.

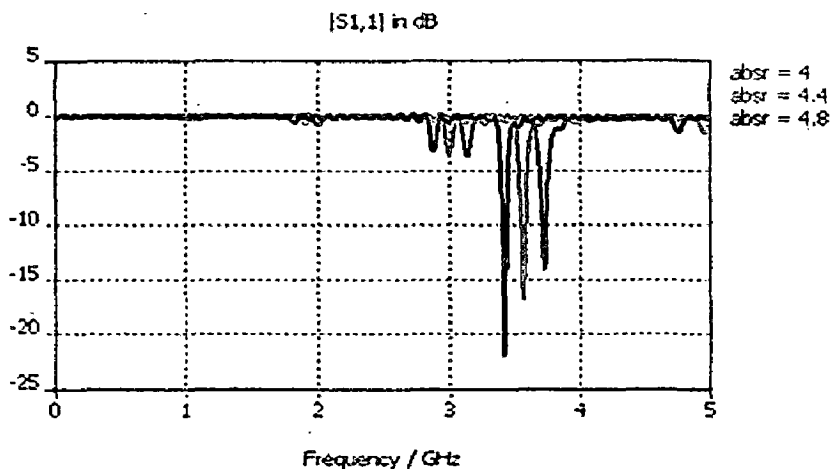


Figure 3.9: Effect of substrate ϵ_r on resonant frequencies of various modes

3.3.4 Effect of probe position

The square ring is fed by a coaxial probe along the diagonal of the ring. The variable r_{pr} as shown in Fig. 3.4 is varied along the diagonal to achieve matching to a 50Ω coaxial probe. It is seen that when feeding is done in the above mentioned way all the modes with frequencies below the TM_{22} mode have return loss worse than -5dB after optimizing the variable r_{pr} . The patch is also fed by a coaxial probe and its position is varied along the central horizontal line to achieve matching.

3.3.5 Effect of substrate

As in a simple microstrip patch antenna resonant frequency of every mode decreases with increase in dielectric constant of substrate. Also bandwidth is increased with decrease in dielectric constant and increase in height [31]. Effect of dielectric constant of substrate on resonant frequencies of various modes is shown in Fig. 3.9

3.5 Fabrication and Measurements

The fabrication has been performed using dry etching technique. There is a shift in resonant frequency observed in both the ports. However this can be attributed to fabrication errors. The measured S parameters on a Vector Network Analyzer are shown in Fig 3.11. The fabricated antenna is shown in Fig. 3.12.

Radiation pattern is measured in the anechoic chamber for both ports operating at their respective frequencies. Fig. 3.13 shows the E plane and H plane farfield patterns of central patch at its resonance frequency. Fig. 3.14 shows the farfield patterns of TM_{22} ring. The patterns are taken in two perpendicular planes XZ and YZ (Axis defined in Fig. 3.4).

3.6 Analysis of the designed antenna

In this chapter the MIMO analysis of the designed antenna is performed. Envelope Correlation Coefficient (ECC) and Mean Effective Gain (MEG) is computed using farfield electric field patterns. Covariance matrix is computed and achievable MIMO capacity using the designed antenna is calculated. Comparison in terms of capacity is made with a 2X1 patch array utilizing spatial diversity. MIMO Antenna Design Suite (Version 1) is developed which is a set of MATLAB programs for obtaining the necessary parameters for evaluating MIMO antenna.

3.6.1 Antenna Covariance

Covariance between i_{th} and j_{th} antennas is defined in Eqn. 3.6.1 below:

$$Cov(i, j) = E\{(V_i - E[V_i])(V_j - E[V_j])^*\} \quad (3.6.1)$$

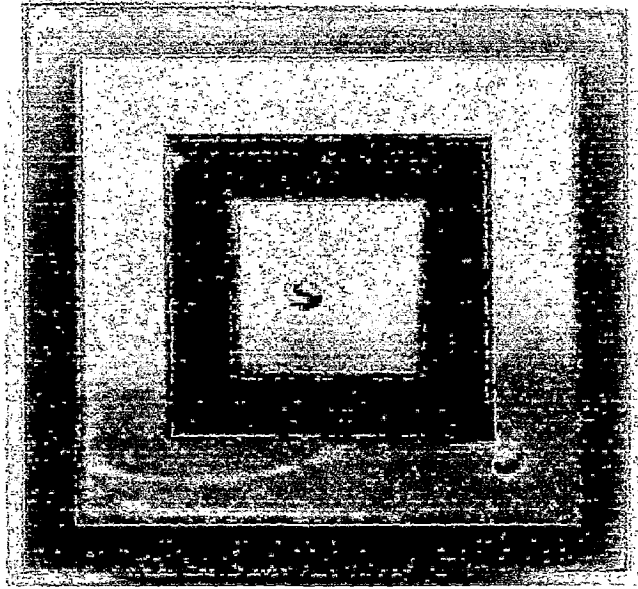


Figure 3.12: Image of the fabricated TM_{22} Square Ring Patch Antenna

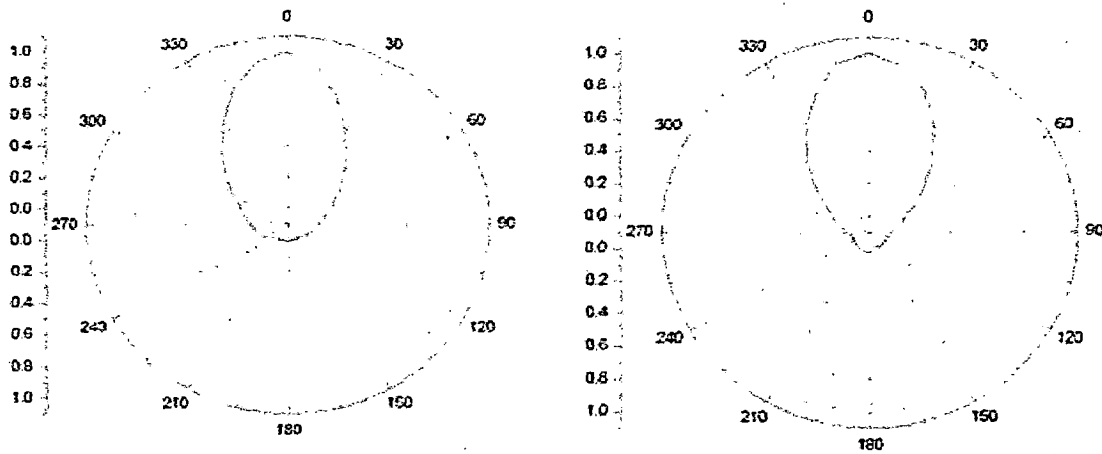


Figure 3.13: (a) E plane farfield pattern of central patch (b) H plane farfield pattern of central patch (In linear scale)

Where K is a constant. XPR is the ratio of time averaged vertical power to time average horizontal power in the fading environment in linear form. XPR is also referred to as the cross-polarization power ratio or cross-polar discrimination (XPD). Both antennas in Eqn. 3.6.4 have E-fields, $E_{\theta n}$ and $E_{\phi n}$ [Vm^{-1}]. $P_{\theta}(\theta, \phi)$ and $P_{\phi}(\theta, \phi)$ are the angular probability density function of incident wave arrival in vertical and horizontal plane respectively. For reference purposes, θ is the angle relative to the vertical axis z and ϕ is the angle in the horizontal plane.

3.6.2 Propagation Channel Model

In mobile wireless communication systems, the transmitted signals are affected by buildings and other obstacles causing reflections, diffraction and scattering leading to multipath environment. The incident radio waves arriving at the mobile terminal antennas have various angles of arrival and XPR. As evident by the correlation equation 2.6.2 mentioned previously, the correlation coefficient is dependent on the multipath environment via the XPR and angular density functions $P_{\theta}(\theta, \phi)$ and $P_{\phi}(\theta, \phi)$.

For simplicity, the angular density function are modelled as product of elevation and azimuth components separately and combined according to:

$$P_{\theta}(\theta, \phi) = P_{\theta}(\theta)P_{\phi}(\phi) \quad (3.6.5)$$

$$P_{\phi}(\theta, \phi) = P_{\theta}(\theta)P_{\phi}(\phi) \quad (3.6.6)$$

In order to evaluate ECC,MEG and covariance matrices, it is necessary to apply a suitable statistical model that is similar to the real environment. In outdoor environment, a uniform distribution can be used to model angular density function in azimuth direction. However in elevation, gaussian distribution was found to be a more reasonable assumption [1]. In indoor environment, generally, uniform azimuth distribution

Where G is a N_T by N_R matrix containing independent identically distributed $CN(0,1)$ elements. R_{Rx} and R_{Tx} are covariance matrices of receive and transmit antennas respectively. Thus R_{Rx} and R_{Tx} include the effect of antenna correlation, while G is purely channel dependent. H is normalized using frobenius norm as follows [13]:

$$\|H_F\|^2 = \sum_{i,j} |H_{i,j}|^2 = N_R N_T \quad (3.6.10)$$

that is

$$H_{norm} = \frac{1}{g} H \quad (3.6.11)$$

Where

$$g^2 = \frac{1}{N_R N_T} \|H_F\|^2 \quad (3.6.12)$$

Thus cumulative distribution function of channel capacity can be obtained using Monte Carlo simulations where G matrix is chosen randomly according to complex gaussian distribution. Here a 2X2 MIMO system is under consideration so R_{Rx} , R_{Tx} and G will be 2X2 matrices. R_{Rx} will be equal to:

$$R_{Rx} = \begin{pmatrix} var(1, 1) & cov(1, 2) \\ cov(2, 1) & var(2, 2) \end{pmatrix} \quad (3.6.13)$$

Similarly R_{Tx} is obtained. The capacity is calculated as follows:

1. Use expression Eqns. 3.6.7 and 3.6.13 to compute the covariance matrices from farfield radiation patterns.
2. Generate identically distributed $CN(0,1)$ elements to create 2X2 G matrix.
3. Calculate H matrix using Eqn. 3.6.9.
4. Normalize H using frobenius normalization according to Eqn. 3.6.10 and keep the value of normalization constant g (from Eqn. 3.6.12).

Capacity". Outage capacity can be found from CCDF curves by evaluating capacity at $1 - P_{out}$.

3.6.4 Results

Envelope Correlation Coefficient

The value of envelope correlation computed from farfield electric field patterns is $3.8403e-005$ which indicates nearly orthogonal channels.

Mean effective gain

Mean effective gain calculated assuming the propagation environment mentioned previously is:

For TM_{22} Square ring port MEG= 0.5089

For TM_{10} central square patch MEG=0.4545

$MEG_1/MEG_2 = 1.1197$ which is very close to unity.

Ergodic and Outage Capacity

A patch array with separation of half wavelength at design frequency of 3.5GHz utilizing spatial diversity is designed for comparison with the designed antenna as shown in Fig. 3.15.

The covariance matrix for TM_{22} ring patch antenna computed using farfield electric field patterns is:

$$R = K' \begin{pmatrix} 29.9907 & 0.1408 - 0.1061i \\ 0.1408 + 0.1061i & 26.9734 \end{pmatrix}$$

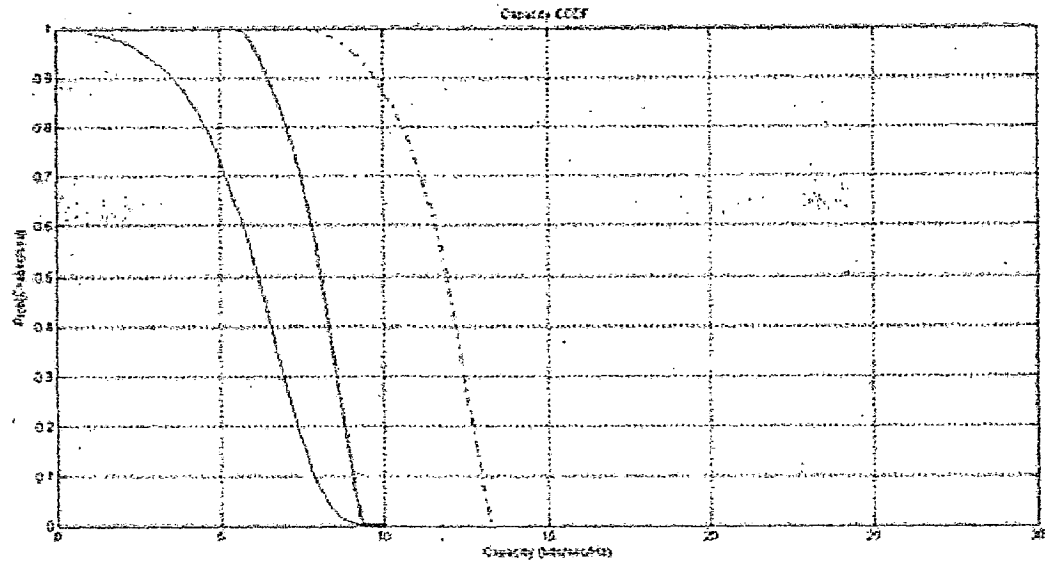


Figure 3.16: Cumulative capacity distribution. (red line shows CCDF of SISO system, blue line shows CCDF of 2X2 MIMO System using designed antenna and Dotted blue line shows the CCDF of 2X2 MIMO System using patch array)

Table 3.2: Capacity comparison for designed antenna with patch array

Capacity	SISO	2X2 MIMO (Designed Antenna)	2X2 MIMO (Patch Array)
Ergodic (in b/s/Hz)	5.9029	7.9022	11.5833
Outage (10%) (in b/s/Hz)	3.5641	6.4781	9.7296

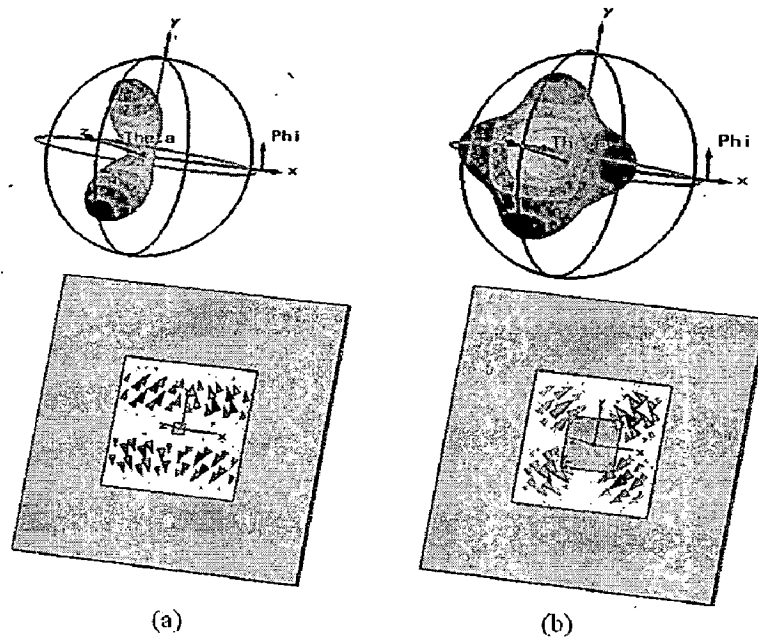


Figure 4.1: Radiation pattern (top) and corresponding surface current distribution (below) of square ring with (a) very less inner gap and (b) as inner gap is increased

and surface current distribution are shown in Fig. 4.1. It can be seen from Fig. 4.1 that when the inner gap is less, the surface current distribution shows a TM_{20} mode and its radiation pattern consists of two lobes. However as the inner gap is increased the surface current distribution of TM_{20} is perturbed leading to decrease in resonant frequency and change in radiation pattern from two lobe pattern to a four lobe pattern as shown in Fig. 4.1. This four lobe pattern has a null in broadside direction and can be successfully used to achieve orthogonality with broadside pattern of a central square patch. Although the TM_{20} mode is disturbed from a two lobe pattern to four lobe pattern with enlargement of inner gap, the square ring will be referred as TM_{20} square ring in the rest of the dissertation. Electric field distribution of this mode is shown in Fig. 4.2.

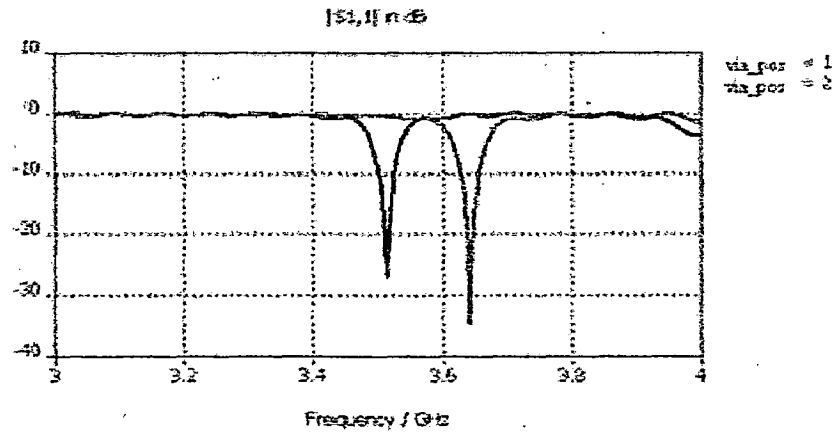


Figure 4.5: Effect of via position on resonant frequency of TM_{20} mode of square ring

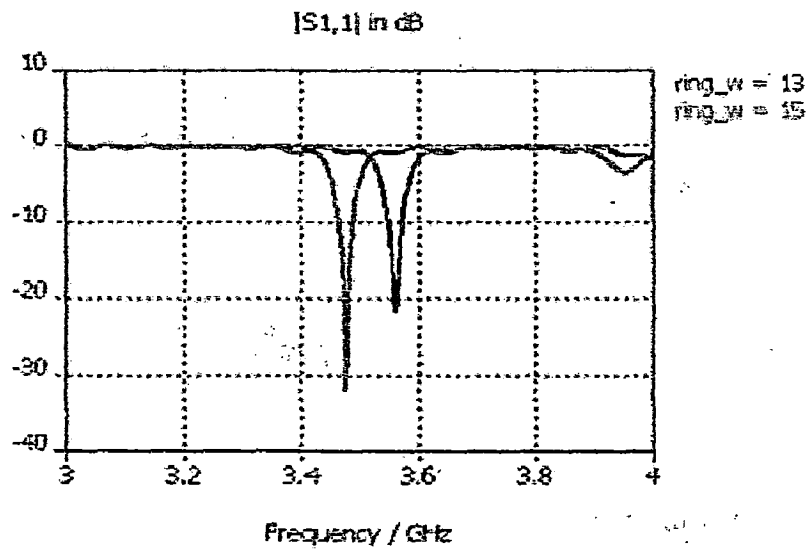


Figure 4.6: Effect of ring width on resonant frequency of TM_{20} mode of square ring keeping via position constant w.r.t. inner edge

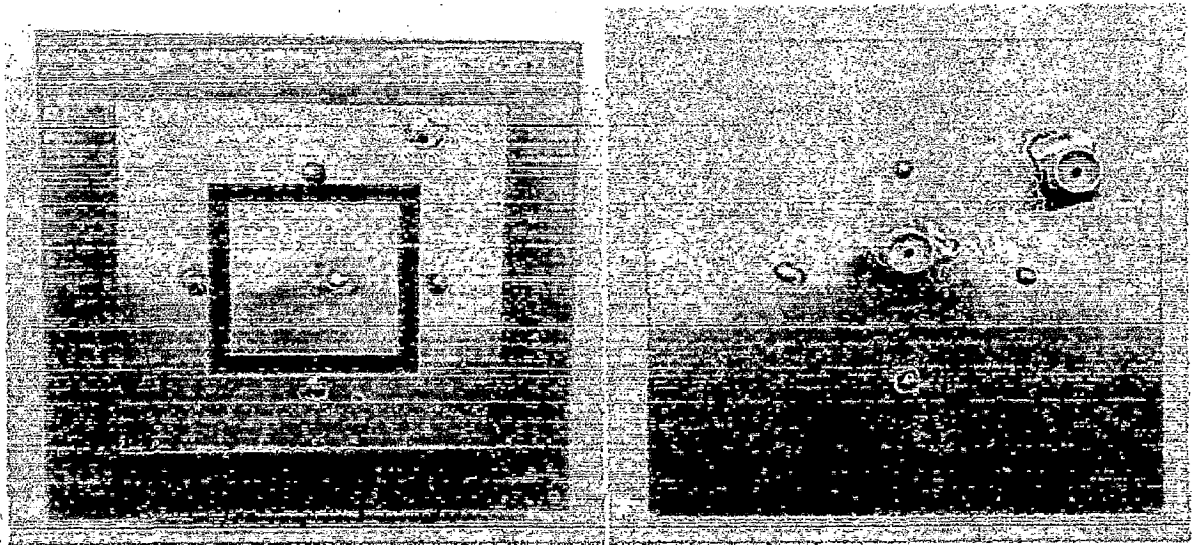


Figure 4.8: Fabricated Square Ring Patch Antenna (front and back sides)

Radiation patterns of the fabricated antenna are shown in Fig. 4.10 and Fig. 4.11.

4.6 Analysis of the Designed Antenna

Envelope Correlation Coefficient

Envelope Correlation Coefficient between ring port and patch port assuming uniform environment: 0.0010

Mean Effective Gain (MEG)

MEG of ring: 0.3398

MEG of patch: 0.4258

The ratio of MEG of both ports 1.2531.

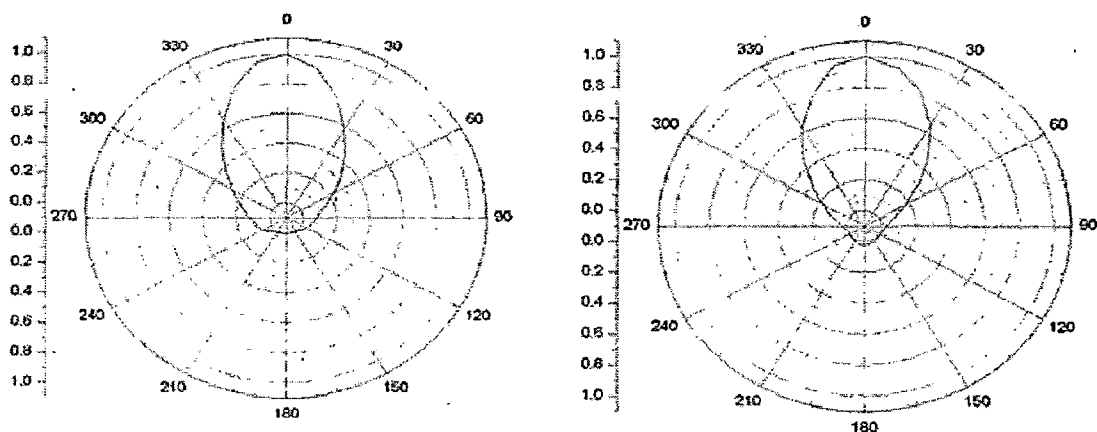


Figure 4.10: (a) E plane farfield pattern of central patch (b) H plane farfield pattern of central patch(In linear scale)

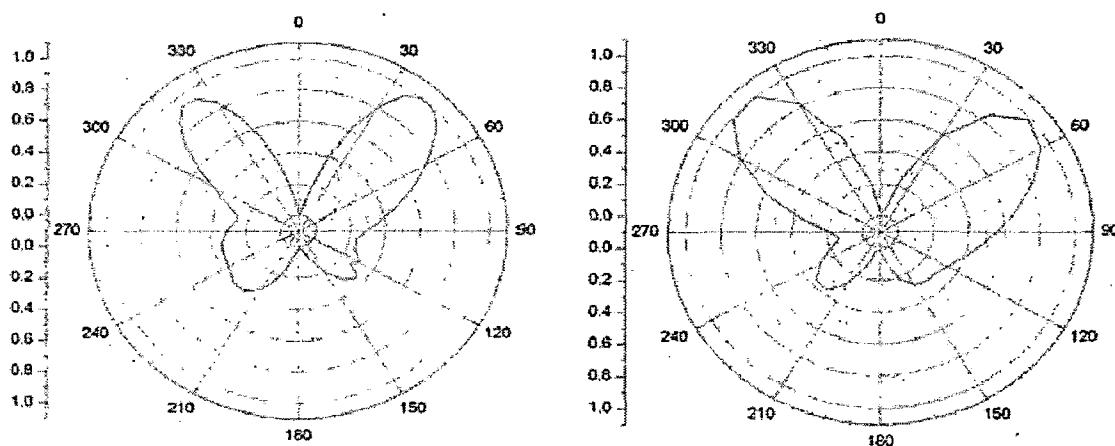


Figure 4.11: (a) Measured farfield gain patterns of TM_{20} ring in XZ plane (b) in YZ plane (In linear scale)

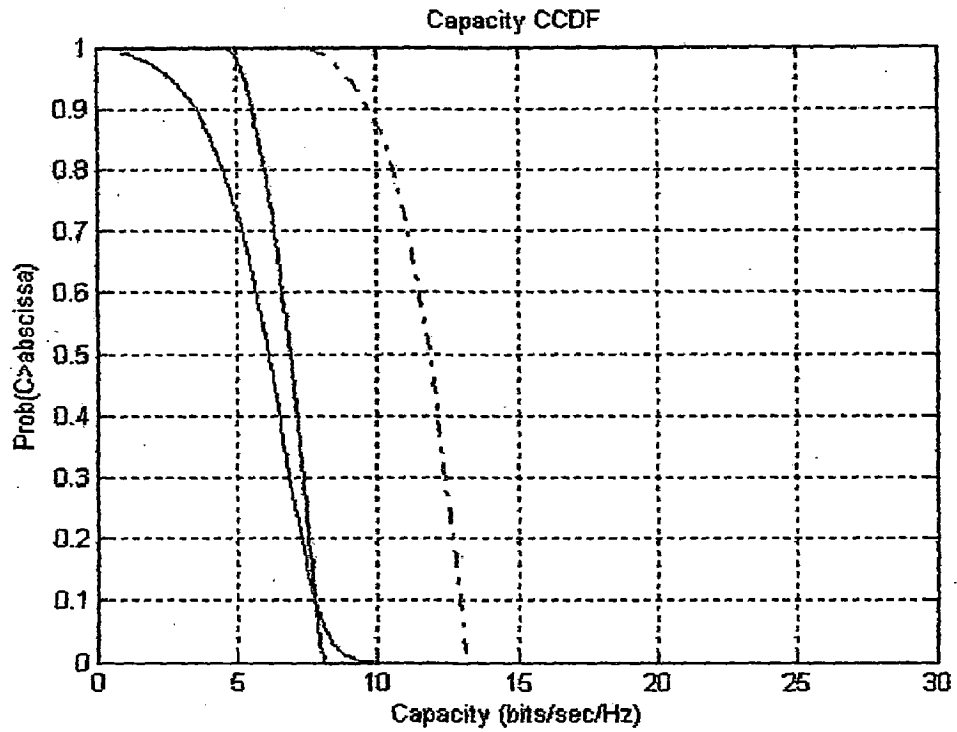


Figure 4.12: Ccapacity CCDF for different cases. (red line shows CCDF of SISO system, Blue line shows CCDF of 2X2 MIMO System using designed antenna and Dotted blue line shows the CCDF of 2X2 MIMO System using patch array)

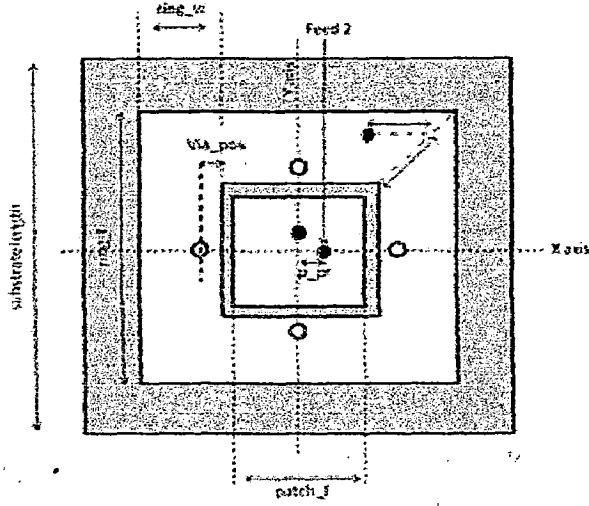


Figure 4.13: 3 port square ring patch antenna

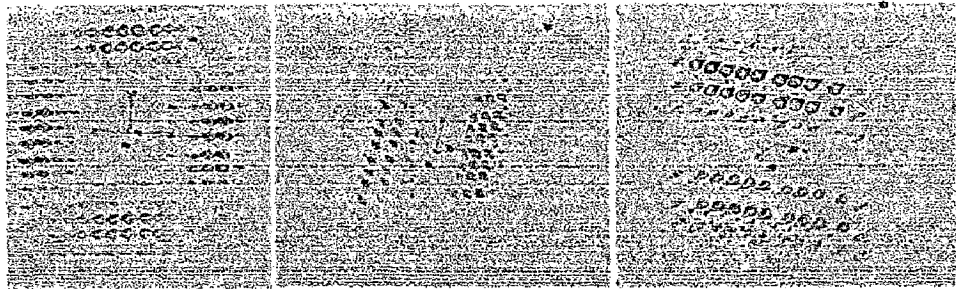


Figure 4.14: E field distribution for different modes in the proposed Square Ring Patch Antenna

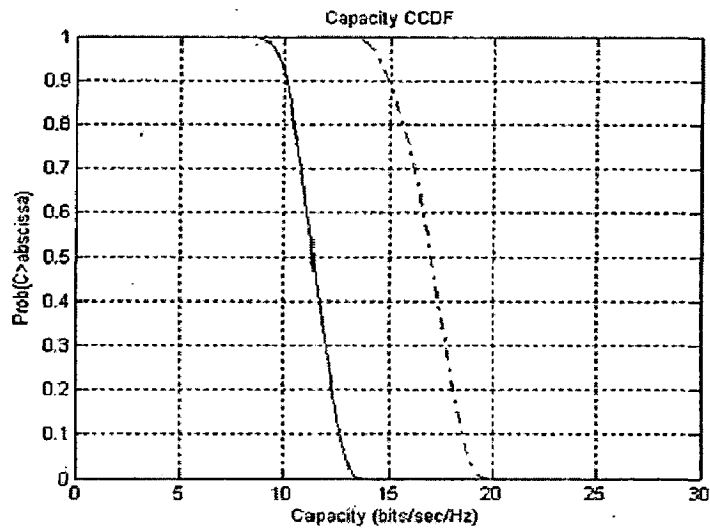


Figure 4.16: CCDF for the designed three port antenna (dotted line represents CCDF of-patch array while solid line represents CCDF of designed antenna)

4.8 Further size reduction of three port square ring patch antenna using patch slots

As shown in Fig. 4.17, the central patch is modified by cutting slots in the shape of x. This concept is taken from [6] and this design results in compactness while maintaining dual polarization feeding. The polarization of antenna is directed at $\pm 45^\circ$ for the two ports. As far as square ring is concerned only two vias are inserted here instead of four in previous case in order to perform size reduction.

Fig. 4.18 shows the radiation patterns of all three ports. it can be seen that using a two via design instead of 4 vias has disturbed the symmetry thus only two lobes instead of four are obtained, thus the pattern has become more directive.

Table 4.3: Optimized values of the design parameters

Parameter	Optimized Value(mm)	Parameter	Optimized Value(mm)
patch_l	16	slot_width	1.0
ring_w	9.192	slot_length	7.3
ring_l	37.76	slot_gap	2
via_pos	0.4	via_r	0.3

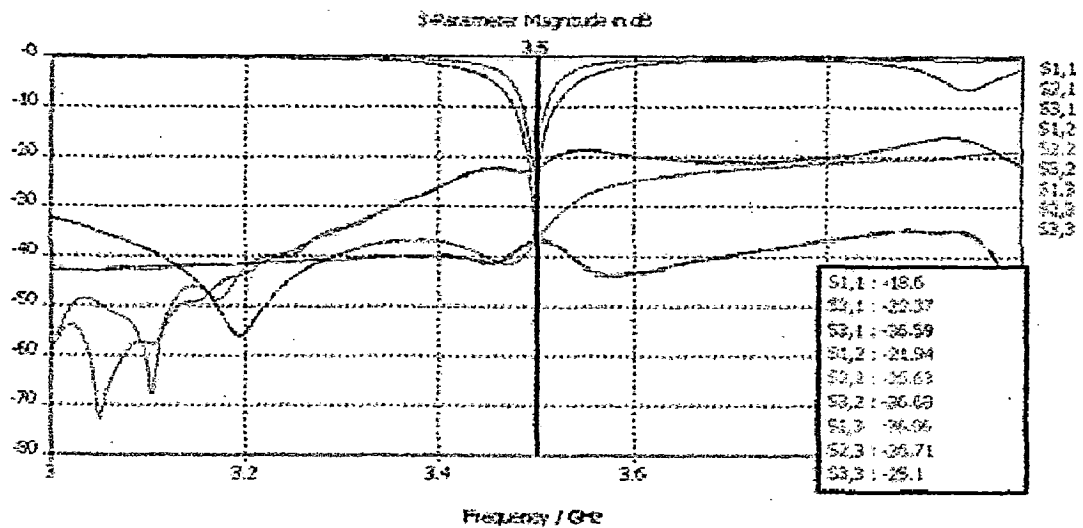


Figure 4.19: Simulated S-parameters of the designed antenna.

4.8.1 Results

The optimized dimensions are given in TABLE 4.3. The simulated S-parameters are shown in Fig. 4.19, which shows mutual coupling less than -20dB in all cases.

Gain of the central patch port 1: 6.8449 dB

Gain of the central patch port 2: 6.8431 dB

Gain of Square Ring port : 6.4532dB

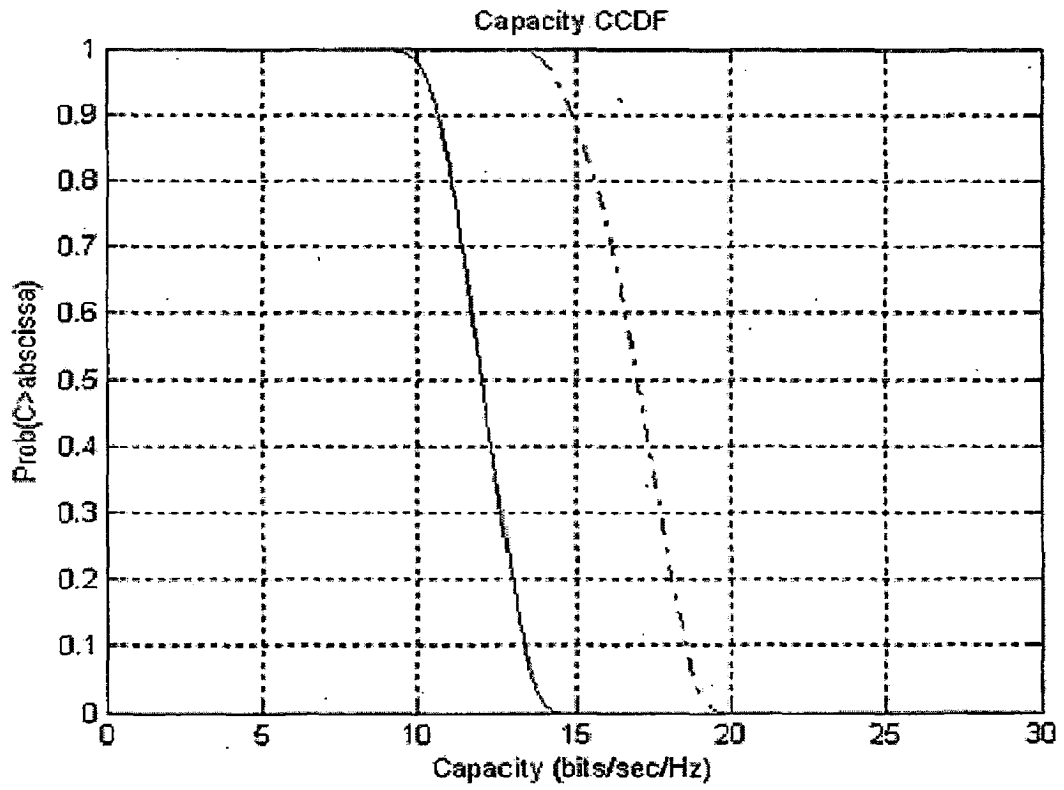


Figure 4.20: CCDF for the designed three port antenna (dotted line represents CCDF of-patch array while solid line represents CCDF of designed antenna)

in lab would be difficult to solder.

TM_{10} (for patch) has been performed. A method for increasing resonant frequency of TM_{20} ring by inserting vias symmetrically in places of high E-field density has been proposed so as to accommodate a central patch. It is seen that an overall size reduction vis-à-vis previous design is obtained. This method can also be used for balancing MEG values of patch and ring ports since increasing size of ring by varying position of vias will increase the top surface area of square ring, thus increasing MEG.

3. Extension to a three port design : orthogonal polarization in central patches can act as two uncorrelated antennas. This concept has been used to add an extra port to the design mentioned in point 2.
4. Further size reduction of three port antenna using X Shaped slots in central patch and removal of two vias from design mentioned in point 3.
5. The analysis in terms of correlation and mean effective gains has been performed for all the designs and results indicate good suitability for MIMO and diversity applications. MIMO Antenna Design Suite (ver. 1) was developed which is a set of MATLAB programs for computing the necessary parameters for evaluating MIMO antennas.

Future scope of this dissertation includes:

1. The propagation environment considered in this dissertation for evaluating correlation and mean effective gain is quite simplified and approximate. Real time testing of the designed antenna using a MIMO testbed can be done. This would incorporate the effects of actual propagating environment. Ray tracing simulations can provide a better insight taking into account and actual propagating

Bibliography

- [1] C. Chiau, "Study of the diversity antenna array for the MIMO wireless communication systems," *PhD thesis, Department of Electronic Engineering, Queen Mary, University of London, United Kingdom, April 2006.*
- [2] R. Vaughan, "Two-port higher mode circular microstrip antennas," *IEEE Transactions On Antennas And Propagation, Vol. 36. No. 3. March 1988.*
- [3] N. Herscovici, C. Christodoulou, E. Rajo-Iglesias, O. Quevedo-Teruel, and M. Sanchez-Fernandez, "Compact multimode patch antennas for MIMO applications," *Antennas and Propagation Magazine, IEEE, vol.50, no.2, pp.197-205, April 2008.*
- [4] C. Waldschmidt and W. Wiesbeck, "Compact wide-band multimode antennas for MIMO and diversity," *IEEE Transactions On Antennas And Propagation, Vol. 52, No. 8, August 2004.*
- [5] J. Sarrazin, Y. Mahe, S. Avrillon, and S. Toutain, "A new multimode antenna for MIMO systems using a mode frequency convergence concept," *IEEE Transactions On Antennas And Propagation, Vol. 59, No. 12, December 2011.*
- [6] J. Sarrazin, Y. Mahe, S. Avrillon, and S. Toutain, "Four co-located antennas for MIMO systems with a low mutual coupling using mode confinement," *Antennas and Propagation Society International Symposium, 2008. AP-S 2008. IEEE, vol., no., pp.1-4, 5-11 July 2008.*

- [17] C. Waldschmidt, C. Kuhnert, T. Fugen, and W. Wiesbeck, "Measurements and simulations of compact MIMO-systems based on polarization diversity," *IEEE Topical Conference on Wireless Communication Technology 2003*.
- [18] F. Adachi, M. T. Feeney, A. G. Williamson, and J. Parsons, "Cross correlation between the envelopes of 900MHz signals received at a mobile radio base station site," *IEE Proceedings Radar and Signal Processing*, vol. 133, no.6 Part F, pp 506-512, Oct 1986.
- [19] S. Saunders, "Antennas and propagation for wireless communication systems," *Wiley, 1999*.
- [20] S. Blanch, J. Romeu, and I. Corbella, "Exact representation of antenna system diversity performance from input parameter description," *IEEE Electronics Letters*, vol.39, pp 705-707, May 2003.
- [21] T. Wittig and V. Sokol, "MIMO antenna simulation," *A Presentation by CST, UGM Darmstadt, 2009*.
- [22] T. Taga, "Analysis for mean effective gain of mobile antennas in land mobile radio environments," *Vehicular Technology, IEEE Transactions on*, vol.39, no.2, pp.117-131, May 1990.
- [23] H. Wang, D. G. Fang, Y. Xi, C. Z. Luan, and B. Wang, "On the mutual coupling of the finite microstrip antenna arrays," *International Symposium on Electromagnetic Compatibility EMC 2007*.
- [24] S. ho Chae, S. keun Oh, and S.-O. Park, "Analysis of mutual coupling, correlations, and TARC in MIMO antenna array," *International Symposium on Antennas and Propagation - ISAP 2006*.
- [25] M. Manteghi and Y. Rahmat-Samii, "Multiport characteristics of a wide-band cavity backed annular patch antenna for multipolarization operations," *IEEE*

- [34] K. Yu., “Modeling of multiple input multiple output radio propagation channels,”
Licentiate Thesis, Royal Institute of Technology, Stockholm, 2002.